Mechanics of Advanced Composite Structures

Journal homepage: https://macs.semnan.ac.ir/

Semnan University

ISSN: 2423-7043

Research Article

Effect Of Nickel Addition on the Coefficient of Thermal Expansion and Microstructural Characteristics of AA2024 and AA7175 Aluminum Alloys in As-Cast and Homogenized States

Rajendra P[a*], Mohan Raju S[a], C M Ramesha[b], R. Chandrashekar[c], Madev Nagaral[d]

[a]*Assistant Professor, Department of Mechanical Engineering, Ramaiah Institute of Technology, Bangalore, 560054, India.*

[a]*Research Scholar, Department of Mechanical Engineering, Ramaiah Institute of Technology, Bangalore, 560054, India.*

[b]*Associate Professor, Department of Mechanical Engineering, Ramaiah Institute of Technology, Bangalore, 560054, India.*

[c]*Professor (Research Consultant or Mentor), Department of Mechanical Engineering, Sambhram Institute of Technology, Bangalore, 560097, India.*

[d]*Manager (Design) Aircraft Research and Design Centre Hindustan Aeronautics Limited, Bangalore-560037, India.*

ARTICLE INFO

Article history:

Received:
Revised:
Accepted:

Keywords:

Aluminum Alloys;
Nickel Micro-Alloying;
Coefficient of Thermal Expansion;
Microstructural Properties;
Stir Casting;
Intermetallic Compounds;
Heat Treatment;
Grain Refinement.

ABSTRACT

Aluminum alloys are widely used in aerospace structures, necessitating continuous improvement in their mechanical properties. Micro alloying with nickel can enhance these properties and improve the coefficient of thermal expansion. This study investigates the influence of nickel on the microstructural and thermal expansion characteristics of AA2024 and AA7175 aluminum alloys, both commonly used in aerospace. AA2024 primarily contains copper, while AA7175 has zinc; both are heat-treatable and possess excellent strength. In this research, alloys were stir-cast with varying percentages of nickel and 0.2% strontium, which improves grain structure. The alloys were homogenized at 480°C for 15 hours, quenched in water, and subjected to tensile testing, EDS, XRD, and microstructural and thermal expansion analyses. Results showed that nickel addition increased strength to 215 MPa for AA2024 and 284 MPa for AA7175 with 5% nickel. XRD and EDS revealed the formation of intermetallic compounds like Al_2Ni_3, Al_3Ni, and Al_3NiCu. However, increasing nickel beyond 5% led to undesirable needle-like structures. Thermal expansion studies indicated a reduction in the coefficient of linear thermal expansion by 14.1% for AA2024 and 16.5% for AA7175 with 2% nickel, reducing thermal stress under loading up to 350°C.

1. Introduction

Aluminum alloys AA2024 and AA7175 are considered the most important materials for use in aerospace components like skins, stringers, and inlet structures of the engine nacelle. The outer structures of the engine nacelle are constructed using the AA2024 alloy, whereas the inner structures are made of AA7175 [1]-[4]. Aluminum alloys are used as a structural member in nacelle structures at a temperature zone of up to 250°C beyond that temperature; titanium

* **Corresponding author.**
E-mail address: *rajendrap@msrit.edu*

Cite this article as:
Rajendra P, Mohan Raju S, C M Ramesha, R Chandrashekar and Madev Nagaral., 2025. Effect of Nickel Addition on the Coefficient of Thermal Expansion and Microstructural Characteristics of AA2024 and AA7175 Aluminum Alloys in As-Cast and Homogenized States. *Mechanics of Advanced Composite Structures*, 12(1), pp. xx-xx
https://doi.org/10.22075/MACS.2024.39315.2050

alloys are preferred since the coefficient of thermal expansion of Ti_6Al_4V is 8.73 µm/m-°C compared with aluminum alloys at 25.2 µm/m-°C at a reference temperature of 350°C [29].

There is a need for improvement in the thermal expansion coefficient of the Al alloys in a thermal environment to reduce their thermal stresses because thermal stresses develop when a component is subjected to thermal loading (Temperature change) when it is constrained. If the element were not constrained, it would be free to displace, with no thermal stress; however, if it is constrained and due to a temperature change, the component expands or contacts based on its thermal expansion property [30]. Structural components used in various applications such as Aircraft engine nacelle, Gas turbines, heat transmission systems [34] [35], power generation plants [36], energy storage, solar cells, supercapacitors [37], high-temperature thermal energy storage (HTES) and parabolic trough collectors (PTC) for solar power generation operating at temperatures 300–550°C [33]. Hence, there is a need to improve mechanical properties, particularly the thermal expansion of the alloy used in the thermal environment for the above-listed structural applications. Aluminum alloys are studied for application at 250°C to 350°C. The mechanical properties of aluminum alloys depend on their alloying elements, which increase their strength due to precipitation hardening [5]-[6]. The strength of an aluminum alloy is influenced by its microstructure, particularly the presence of metastable precipitates within the matrix [7].

In this research work, the most used aluminum alloys, AA2024 and AA7175, as structural members in aerospace are selected and modified by adding a varying Ni% to enhance its strength and slightly adding strontium to improve its grain structure, thereby trying to achieve improved mechanical strength and coefficient of thermal expansion, which helps us to select aluminum alloys in a thermal environment in the temperature range of 250°C to 350°C. Nickel is chosen for the present study as nickel helps in improving the coefficient of thermal expansion and mechanical properties of aluminum alloys [7]-[11].

1.1. Influence of Nickel in Aluminum Alloy

Various alloying elements are added to aluminum alloys to enhance their mechanical and metallurgical properties [8]. It is known that Copper and magnesium increase the hardness and strength of aluminum alloys; however, Copper reduces stress corrosion but increases susceptibility to stress corrosion cracking. To counter this, nickel is often added to copper alloys, as it improves high-temperature properties, lowers the coefficient of thermal expansion, further improves cast-ability, and competes with mainstream casting materials such as Al-Si alloys [7]-[11].

Eutectic phases Al_3Ni, Al_9FeNi forms solid solution with Al-Si-Mg, Al-Zn-Mg-Cu, Al-Cu-Si-Mg, Al-Mg-Zn, Al-Mg, matrix [7]. Adding nickel to aluminum alloys by nickel to aluminum alloys up to 4% by weight increases the density of aluminum alloy from 2.70 g/cm^3 to 2.78 g/cm^3 [12].

1.2. Phase Diagram of Nickel & Aluminum Binary Alloy

The Aluminum Nickel phase diagram comprises four different intermetallic compounds, as shown in Fig. 1, which include Ni2Al3, NiAl3, Ni3Al, and NiAl. NiAl forms at 50% atomic weight and the other three compounds form via peritectic reactions. Intermetallic phase $NiAl_3$ forms at 860°C at 28%Ni, and Ni_2Al_3 forms via peritectic reaction at 59%Ni. It is a trigonal with five atoms per unit cell [9, 10]. At the eutectic temperature, 20.2% aluminum can be dissolved in the nickel solid solution. Bletry has studied the rapid solidification of Al-Ni alloys and obtained a super-saturated solid solution of Aluminum with 5% Ni through a splat cooling device.

Similarly, Tonejc et al. further improved the solid solubility of nickel in aluminum by up to 7.7%Ni using smaller samples and employing the "two-piston" technique. Rapid solidification has not been able to increase the solid solubility of nickel in aluminum at concentrations of more than 8%Ni [9].

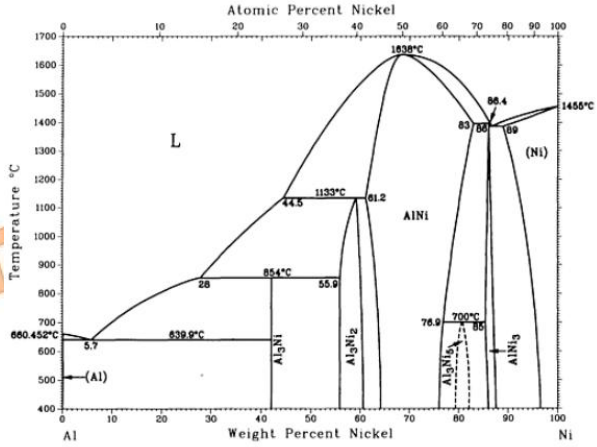

Fig. 2. Aluminum Nickel binary phase diagram [13].

1.3. Influence of Strontium Additions to Aluminum Alloy

The addition of rare earth metals transitions elements like Sc, Hf, and Zr to aluminum, which leads to changes in the grain structure of aluminum alloys, as shown in Fig. 2. These

elements act as intermetallic precipitate that refines the grains by preventing grain boundary migration [14]-[16]. Strontium (Sr) additions of up to 0.05 wt% in aluminum alloys result in significant grain refinement and reduced porosity, particularly in Al-Si alloys. In 319, aluminum alloy castings added with Sr improved ultimate tensile strength to 215 MPa. Sr also enhances the corrosion resistance of A356 alloys. The Al-Sr phase diagram shows that Al_4Sr melts at 1025°C as shown in Figure 2, Al_2Sr forms peritectically at 920°C, and a complex BCC AlSr structure forms at 80 wt% Sr [17]-[21].

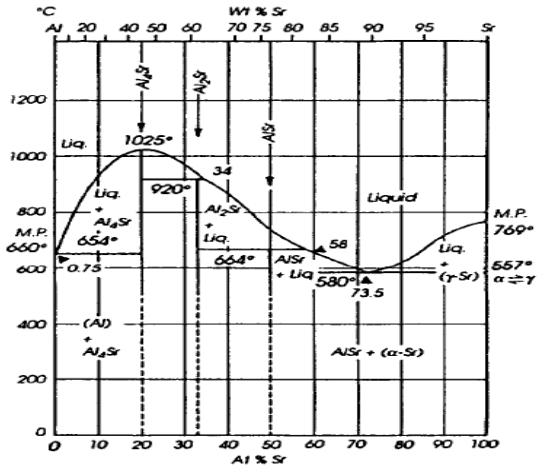

Fig. 2. Aluminum Strontium phase diagram [22]-[23].

This research aims to assess the impact of nickel additions in aluminum alloys AA2024 and AA7175 and to study the influence of homogenization on nickel-enhanced alloys. The investigation involves comprehensive analysis using various techniques, including Optical Microscopy (OM), Scanning Electron Microscopy (SEM), X-ray Diffraction (XRD), Energy Dispersive X-ray Spectroscopy (EDS), and thermal expansion studies.

2. Experimental Details

The Aluminum alloys AA2024 and AA7175 were stir-cast by adding varying percentages of nickel (0%, 0.04%, 0.08%, 2%, 5%, and 10 %Ni) and 0.2% strontium. Nickel powder with a particle size of <50µm is added, and Strontium is added by adding a calculated amount of Al-10%Sr Master Alloy to the Aluminum charge in the crucible. The stir-cast Aluminum alloys are then homogenized in an electric furnace at 480°C for up to 15 hours and then quenched in water.

Preparing a smooth surface is essential for accurately capturing microstructures, which can be accomplished using a polishing machine. The samples, machined to standard dimensions of 25 mm x 25 mm x 5 mm, were prepared for microstructural analysis, shown in Fig. 3 and Fig. 4. These identical specimens were used for various tests, including optical microscopy, scanning electron microscopy (SEM), X-ray diffraction (XRD), and energy-dispersive spectroscopy (EDS). The microstructures of both as-cast and homogenized specimens of AA2024 and AA7175 alloys were examined using a scanning electron microscope, as depicted in Fig. 5, with the equipment sourced from IISC.

Fig. 3. Polished samples for microstructure examination

Fig. 4. Specimens are placed in a specimen holder, and Desiccator

Fig. 5. ZEISS ULTRA 55 SEM (Gemini Technology) from IISc.

2.1. XRD Analysis:

The samples prepared for microstructural analysis were also subjected to XRD analysis. The specific parameters used for the XRD examination are outlined in Table 1, and the device is shown in Fig. 6.

Table 1. Parameters for XRD Analysis

Sl. No.	*Parameter*	*Specifications*
1	Maximum measurement diameter	250 mm
2	Minimum angular step size	0.0001º
3	Maximum rotation speed	1500º /min
4	Theta angular range	-5 ºto 40º
5	2Theta angular range	-10º to 60º
6	Measurement reproducibility	+/- 0.0001º

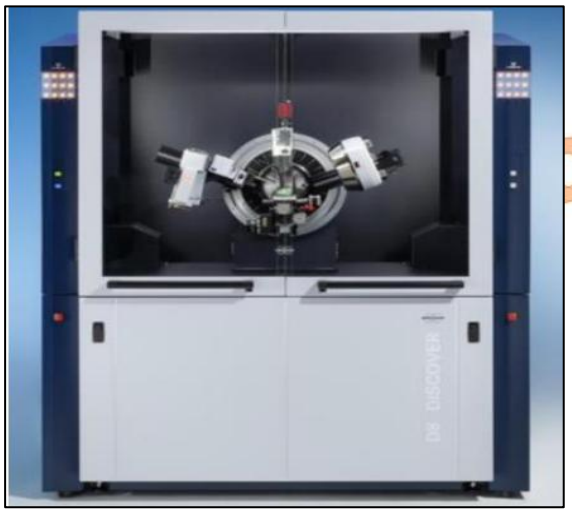

Fig. 6. *XRD D8 Machine for XRD analysis.*

2.2. Thermo-Mechanical Analysis

Thermo-mechanical analysis was performed at CPRI using the TA-Instruments Q400 TMA. This test measures a material's thermal expansion by observing changes in length as temperature increases. The test was conducted on 10 mm cube specimens from micro-alloyed (0.08% Ni) and macro-alloyed (2% Ni) groups of modified AA2024 and AA7175 alloys, selected based on tensile and microstructural results. Five specimens per sample were tested, as indicated in Fig. 7, and the expansion was measured up to 350°C to calculate the thermal expansion coefficient using Equation 1. The parameters are provided in Table 2.

$$\frac{\Delta l}{l_o} = (\alpha \times \Delta t) \quad (1)$$

where

Δl = Change in length (mm)

lo = Original length (mm)

α = Coefficient of thermal expansion

Δt = Temperature change (°C)

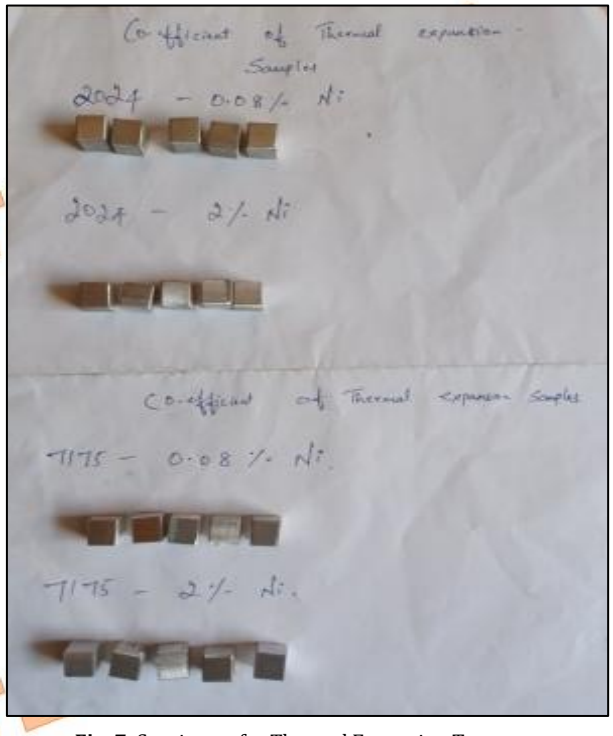

Fig. 7. Specimens for Thermal Expansion Test.

Table 2. Selection of samples for thermal expansion test.

Alloy % range	% of Ni added	Thermal expansion Test	Remarks
Base Alloy	0% Ni	No	Since Base alloy thermal expansion is known from Reference MMPDS [S11]
Micro Alloyed Nickel %	0.04% Ni	No	Considered 0.08%, rather than 0.04% Ni, since we have almost the same result in a tensile test
	0.08% Ni	Yes	
Macro Alloyed Nickel %	2.0% Ni	Yes	Considered 2.0 % Ni since microstructure and tensile test results were better.
	5.0% Ni	No	
	10.0% Ni	No	Since the result from the tensile test shows high brittleness

3. Results and Discussions

3.1. Tensile Test Results

AA2024 alloy varying Ni%: The tensile strength of nickel-added AA2024 aluminum alloy showed varied results depending on the nickel content. Micro-alloyed samples with 0.04% and 0.08% nickel exhibited a minor strength increase, ranging between 12 to 15 MPa. In contrast, macro-alloyed samples containing 2% and 5% nickel significantly improved, as shown in Fig. 8, with tensile strength reaching 215.7 MPa. However, when the nickel content decreased due to increased brittleness was increased to 10%, the alloy's strength

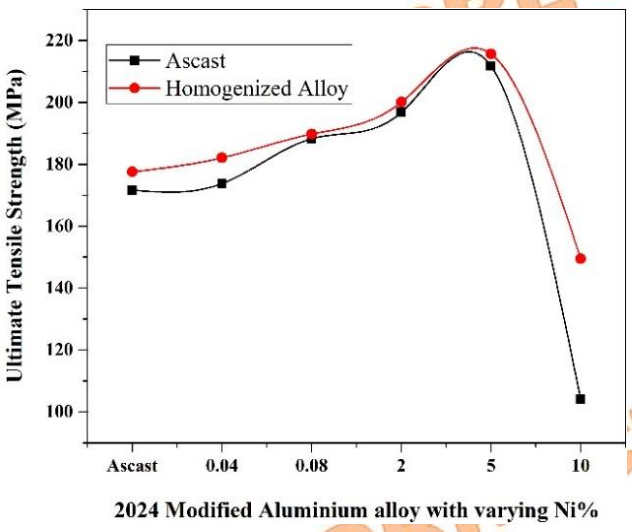

Fig. 8. AA2024 with various Ni% at as-cast, Homogenized.

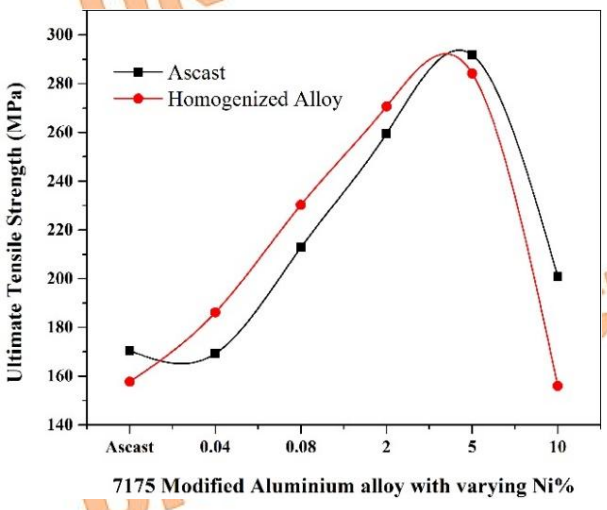

Fig. 9. AA2024 with various Ni% at as-cast, Homogenized

AA7175 alloy varying Ni%: The addition of varying Ni% to AA7175 aluminum alloy led to a noticeable improvement in ultimate tensile strength. A significant increase from 157.7 MPa to 284.2 MPa was observed for the homogenized AA7175 alloy. Micro-alloyed nickel additions (0.04% and 0.08%) resulted in a strength increase of nearly 60 MPa. In comparison, macro-alloyed samples (2% and 5% nickel) showed strength gains up to 290.4 MPa in Fig. 9. However, adding 10% nickel caused a decline in tensile strength due to brittleness, similar to the trend in AA2024 alloy. This improvement in tensile strength helps select alloys capable of withstanding higher loads for aircraft structural applications [31].

In comparing AA 2024 and AA 7175 alloys with Nickel (Ni) additions, AA 7175 consistently shows higher tensile strength than AA 2024. For 2% Ni additions, AA 7175 achieves a tensile strength of 270 MPa, while AA 2024 reaches 200 MPa. With 5% Ni, AA 7175 achieves 284 MPa compared to 215 MPa for AA 2024. The difference in tensile strength between as-cast and homogenized conditions is minimal for both alloys.

3.2. Microstructural Results

Optical Microstructures were determined at 100X and 100 µm and shown in Fig. 10 and Fig. 11 for AA 2024 and AA7175 with varying % of Ni at homogenized and forged conditions, respectively. Similarly, SEM images were determined at 350X, 20.0 KV, and shown in Fig. 12 and Fig. 13.

As-cast structures exhibit coarse grains in AA 2024 alloys with varying Nickel (Ni) content, while adding up to 2% Ni refines the grain boundaries into fine, equiaxed structures; beyond 2% Ni, needle-like structures form, particularly with 5% and 10% Ni additions. Intermetallic grains begin to form at 2% Ni, influencing the grain boundary characteristics as shown in Fig. 10 and Fig. 11.

In AA 7175 alloys, as-cast and low Ni additions (0.04%) show coarse grains, while 0.08% Ni additions lead to equiaxed grain boundaries. They added up to 2% Ni, resulting in fine grains due to the formation of intermetallic dispersoids. Like AA 2024, 5% and 10% Ni additions produce needle-like precipitates. Overall, both alloys demonstrate grain refinement with Ni additions up to 2%, with more pronounced intermetallic and needle-like structures at higher Ni levels, as shown in Fig. 12 and Fig. 13.

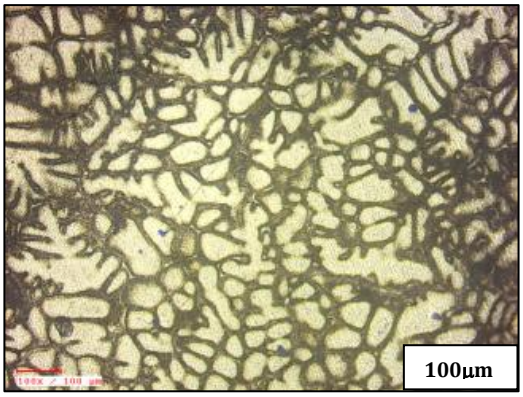

(a) As-cast Homogenized

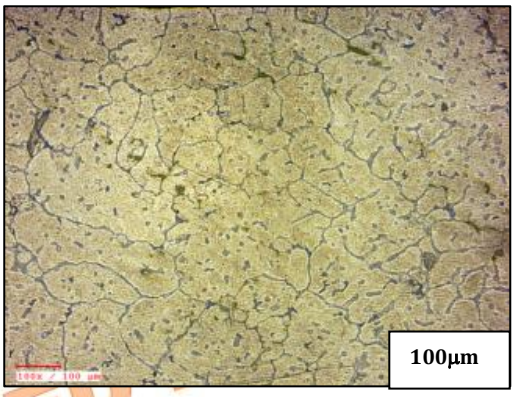

(b) As-cast Forged

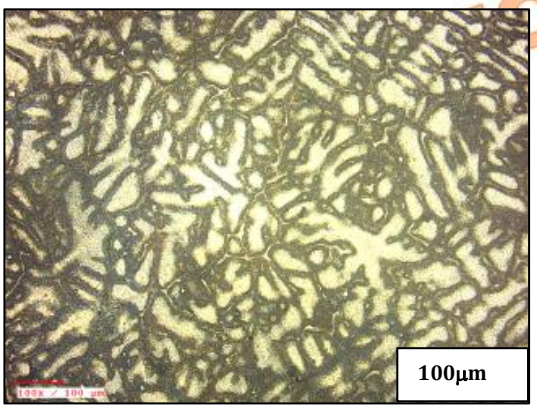

(c) 0.04%Ni +0.2%Sr HC

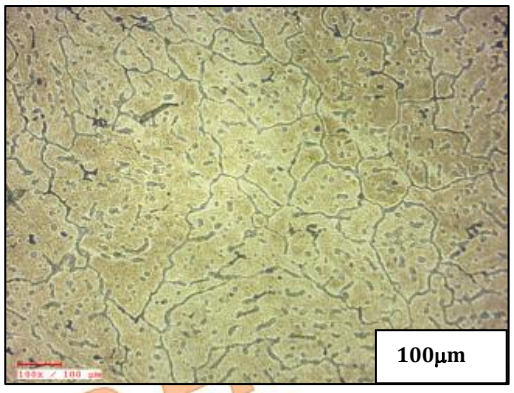

(d) 0.04%Ni +0.2%Sr FC

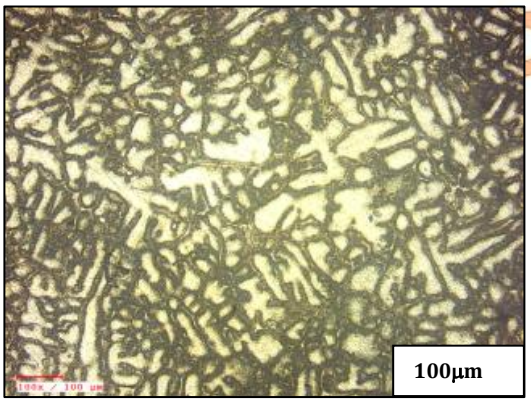

(e) 0.08%Ni +0.2%Sr HC

(f) 0.08%Ni +0.2%Sr FC

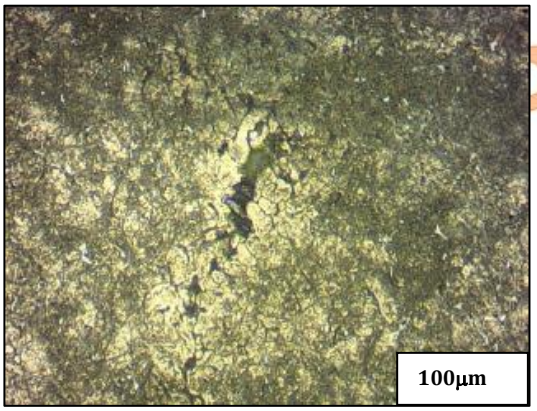

(g) 2%Ni +0.2%Sr HC

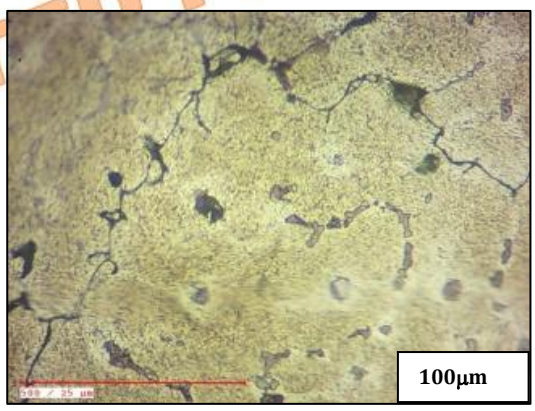

(h) 2%Ni +0.2%Sr FC

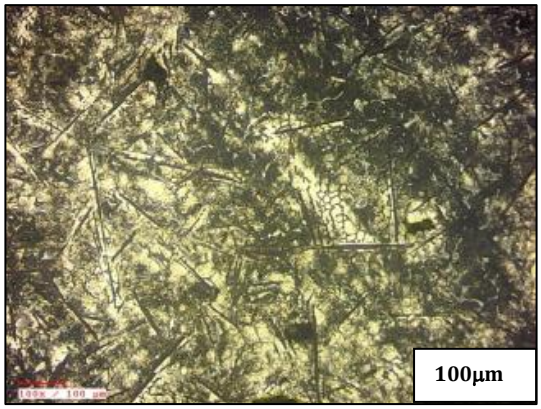

(i) 5%Ni +0.2%Sr HC

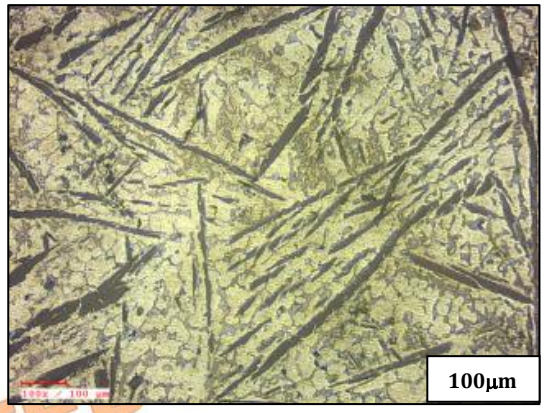

(j) 5%Ni +0.2%Sr FC

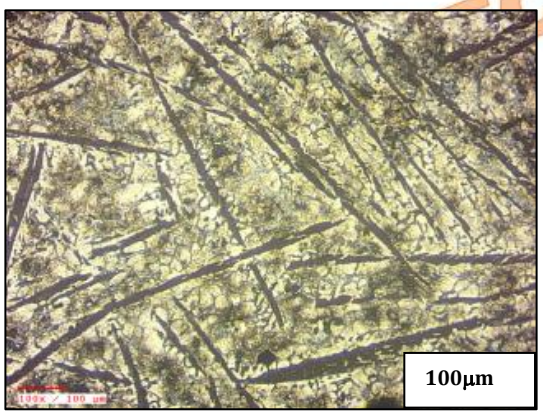

(k) 10%Ni +0.2%Sr HC

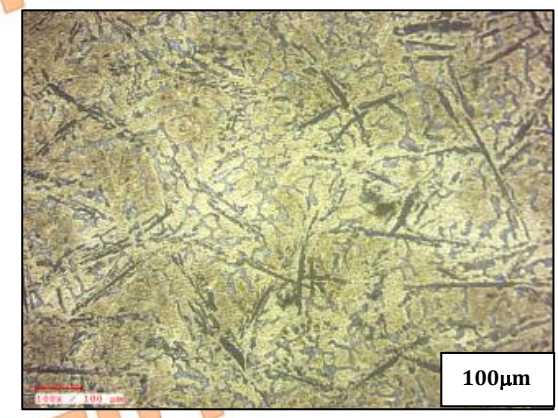

(l) 10%Ni +0.2%Sr FC

Fig. 10: Optical Microstructures (100X / 100 µm) of **AA2024** with added varying Ni% and 0.2% of Strontium (Sr) in Homogenized condition (HC) and Forged condition (FC)

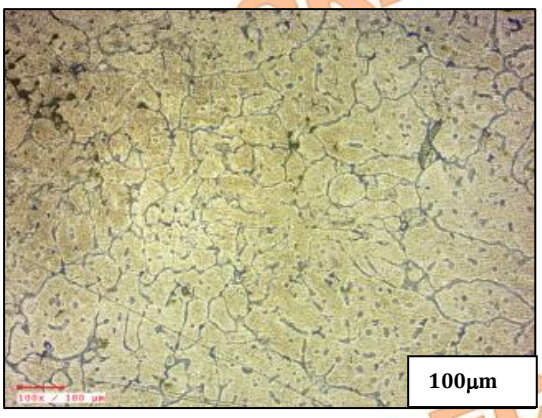

(a) As-cast Homogenized

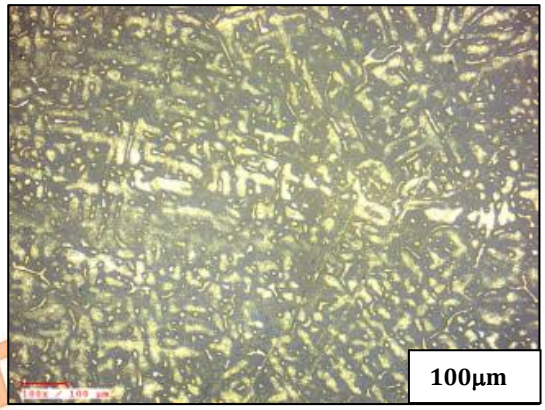

(b) As-cast Forged

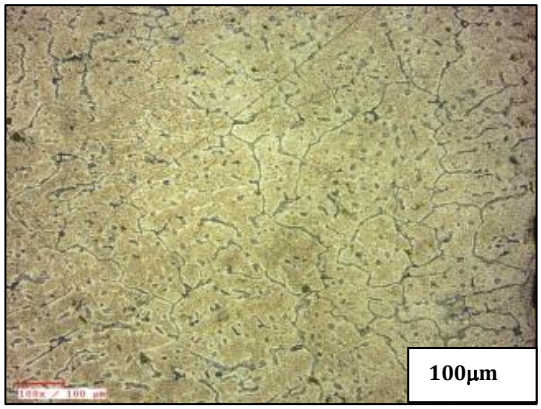

(c) 0.04%Ni +0.2%Sr HC

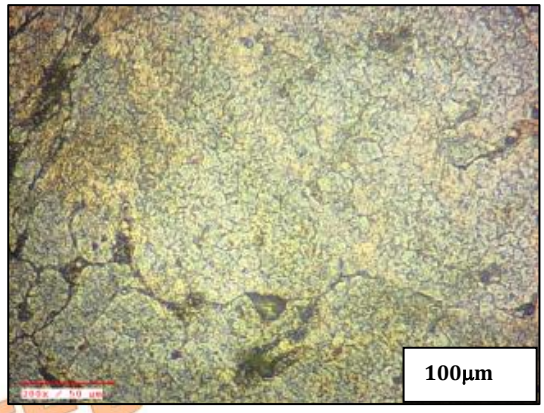

(d) 0.04%Ni +0.2%Sr FC

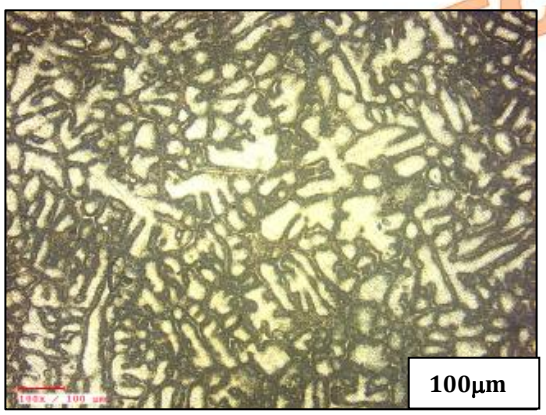

(e) 0.08%Ni +0.2%Sr HC

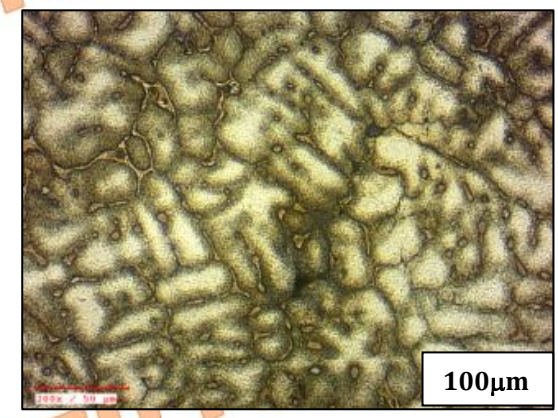

(f) 0.08%Ni +0.2%Sr FC

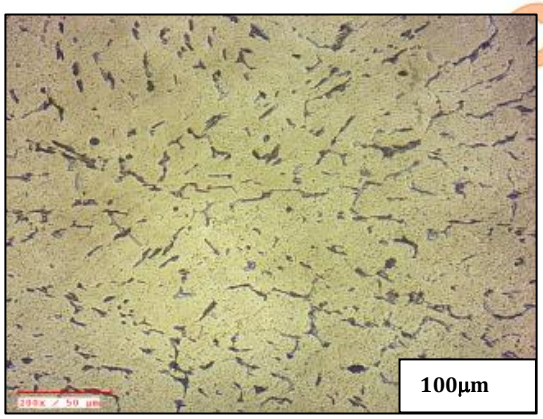

(g) 2%Ni +0.2%Sr HC

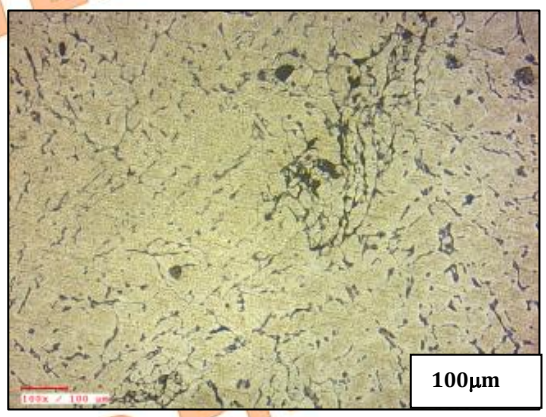

(h) 2%Ni +0.2%Sr FC

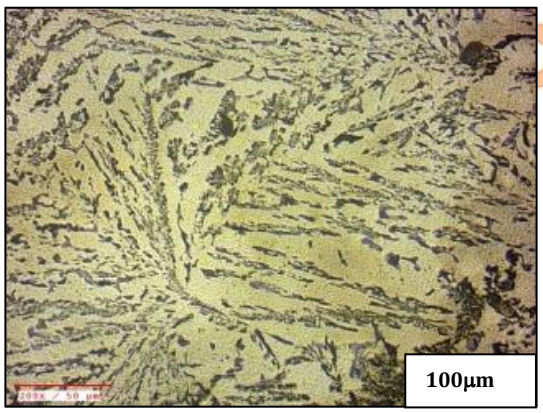

(i) 5%Ni +0.2%Sr HC

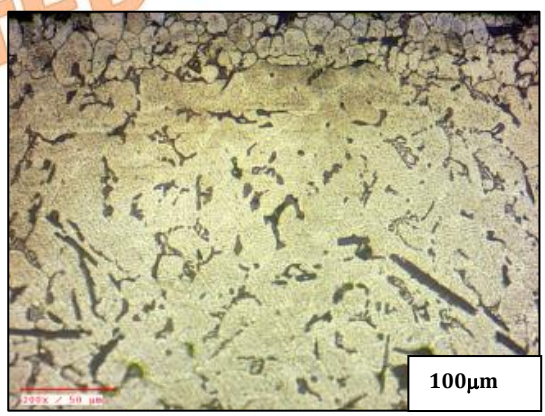

(j) 5%Ni +0.2%Sr FC

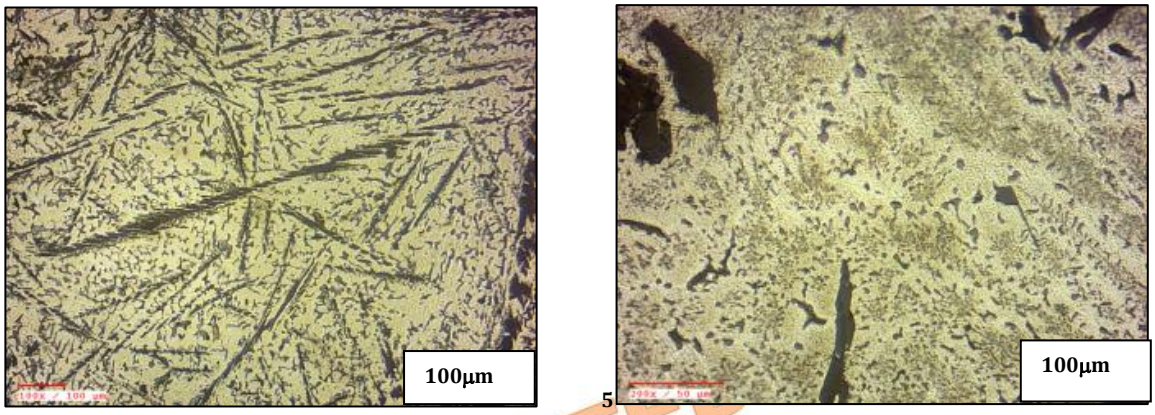

(k) 10%Ni +0.2%Sr HC **(l) 10%Ni +0.2%Sr FC**

Fig. 11: Optical Microstructures (100X / 100 µm) of AA**7175** with added varying Ni% and 0.2% of Strontium (Sr) in Homogenized condition (HC) and Forged condition (FC)

The SEM results shown in Fig. 12 and Fig. 13 exhibit dendritic structures. The formation of intermetallic structures like Ni_2Al_3, NiAl, and NiAl3 due to the addition of Nickel in 0.04% and 0.05% Ni alters this dendritic structure and forms fine grains up to 2% Ni addition and increase in Nickel content increases the amount of Eutectic phase. Above 2% Nickel addition, fibrous or needle-like intermetallic structure Al3Ni is formed, revealed in 5% and 10% Ni addition SEM images.

SEM images for the forged condition show a dense formation of fibrous/needle for 5% and 10% Ni additions, Which is slightly higher than the As-cast and homogenized conditions. This is due to the increased percentage of Ni_2Al_3 intermetallic structures, which decreases elongation and makes them brittle. SEM images shown in Fig. 14 and Fig. 15 are for AA7175 alloy added with varying % of Nickel at As-cast, Homogenized, and Forged conditions. There is not much variation compared to AA2024 alloy shown in Fig. 12 and Fig. 14. No grains were observed for 0%Ni, and 0.04%Ni added alloy, grains formed in 0.08% and fine grains were observed for 2%Ni, with the formation of fibrous structures for 5% and 10%Ni AA7175.

The homogenized alloys showed structures similar to those in the As-cast condition. No grains were formed for 0%Ni, 0.04%, and 0.08% Ni additions. It is observed with small or few grains for 2% with very little porosity. Uniform grains were seen for 5% Nickel additions; for 10%Nickel additions, fibrous inter-metallic structures were formed. In the forged state, the microstructures were similar to as-cast and homogenized conditions; however, the only difference is that fine grains were formed for 0.08% Nickel additions rather than 2% Nickel additions. The EBSD could also offer a more detailed understanding of crystallographic texture and grain boundary misorientation, which are critical for predicting material behavior. These aspects will be explored in greater detail in future work.

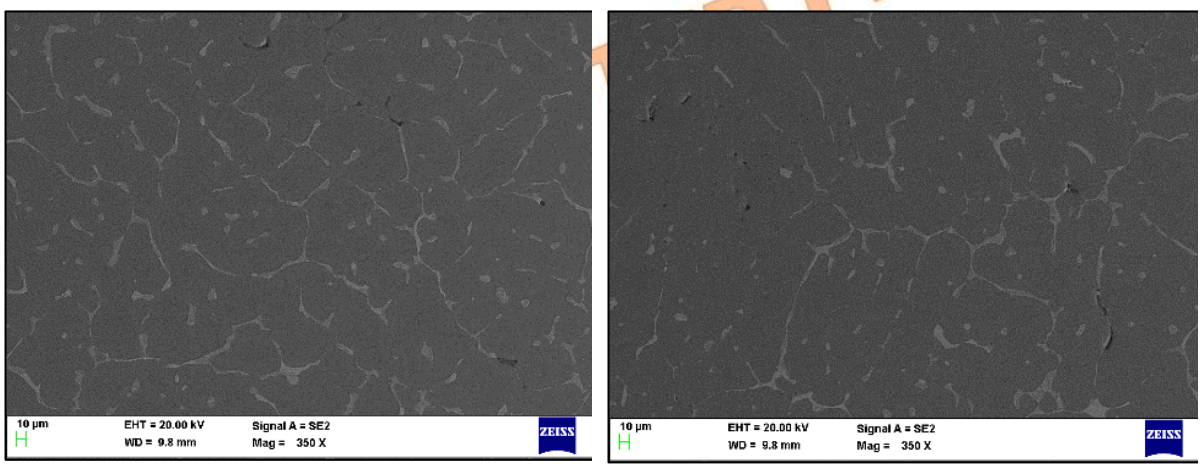

(a) AA 2024 As-cast (b) AA 2024 + 0.04%Ni +0.2%Sr

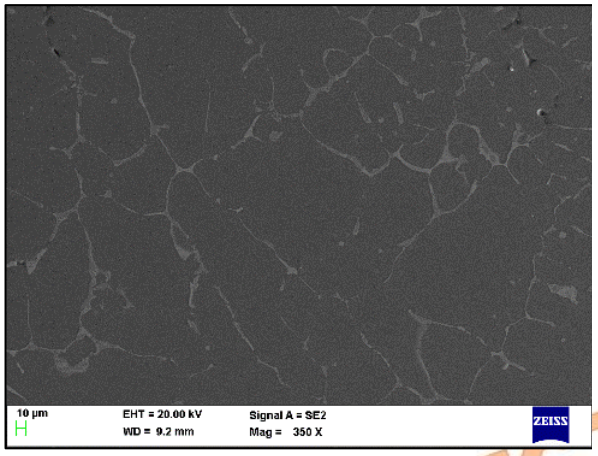

(c) AA 2024 + 0.08%Ni +0.2%Sr

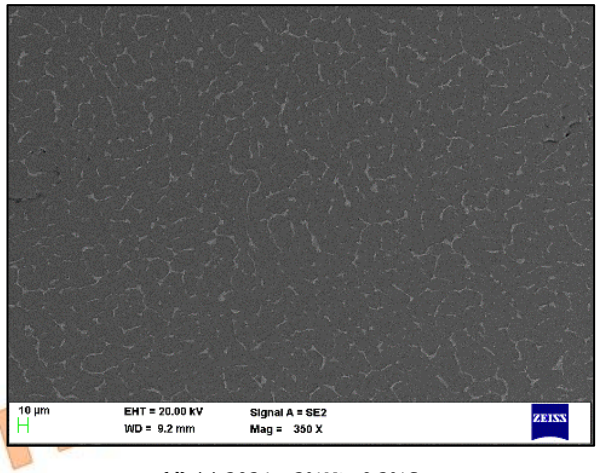

(d) AA 2024 + 2%Ni +0.2%Sr

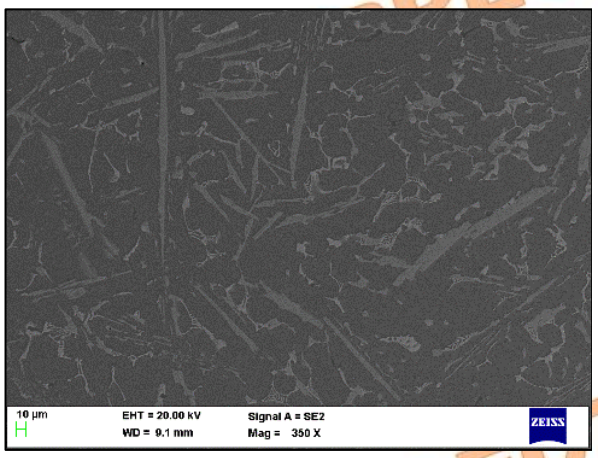

(e) AA 2024 + 5%Ni +0.2%Sr

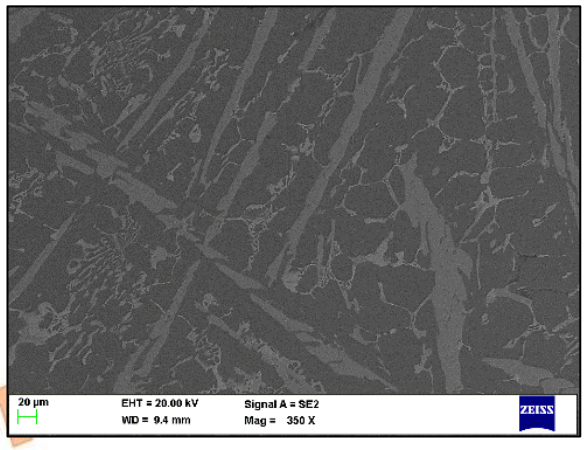

(f) AA 2024 + 10%Ni +0.2%Sr

Fig. 12. SEM Microstructures (350X, 20.0 KV) of **AA2024** with added varying Ni% and 0.2% of Strontium (Sr) in As-cast condition (AC)

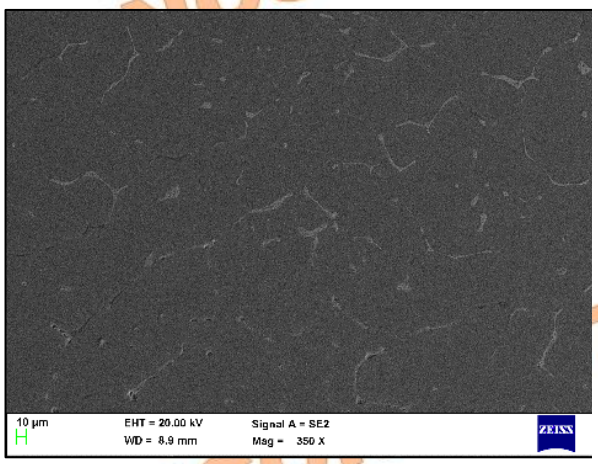

(a) AA 7075 As-cast

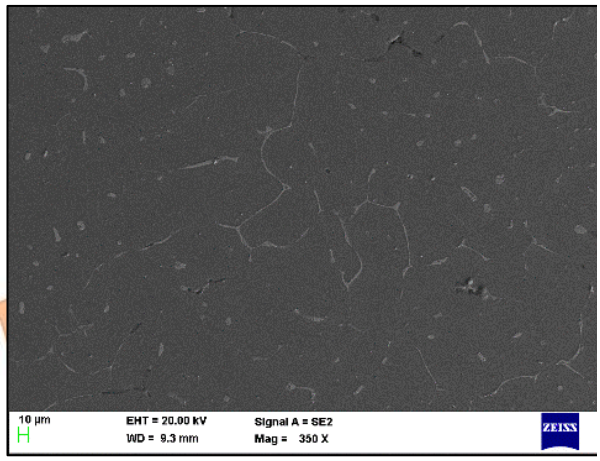

(b) AA 7075 + 0.04%Ni +0.2%Sr

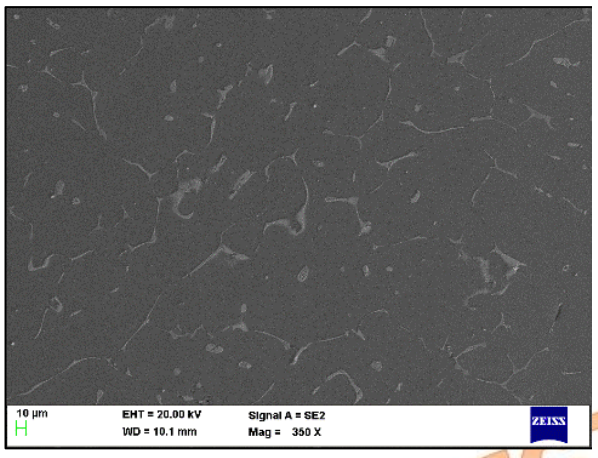

(c) AA 7075 + 0.08%Ni +0.2%Sr

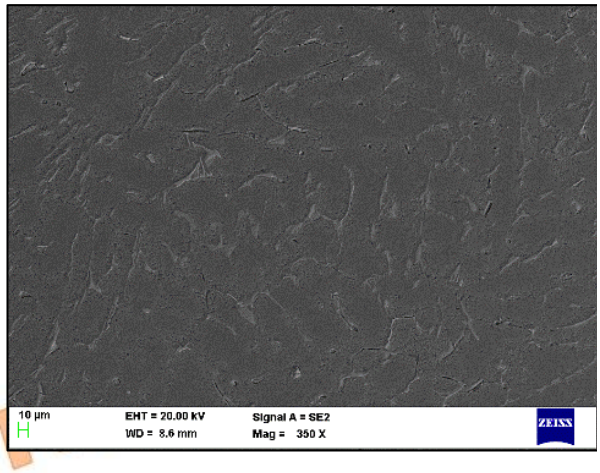

(d) AA 7075 + 2%Ni +0.2%Sr

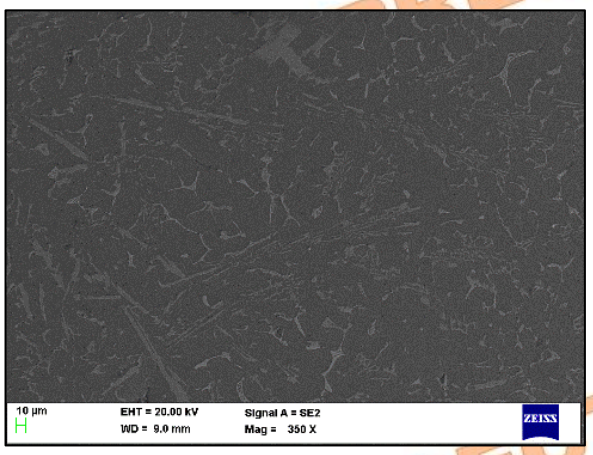

(e) AA 7075 + 5%Ni +0.2%Sr

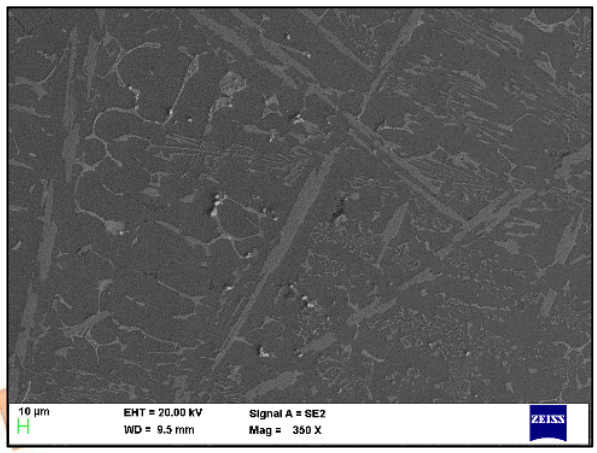

(f) AA 7075 + 10%Ni +0.2%Sr

Fig. 13. SEM Microstructures (350X, 20.0 KV) of **AA 7175** with added varying percent of Nickel (Ni) and 0.2% of Strontium (Sr) in As-cast condition (AC)

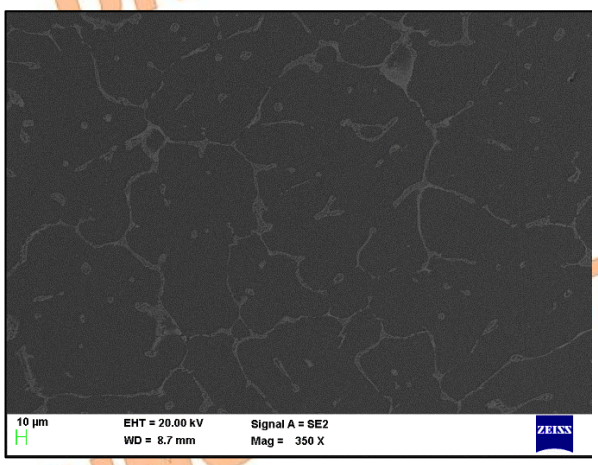

(a) As-cast **Homogenized**

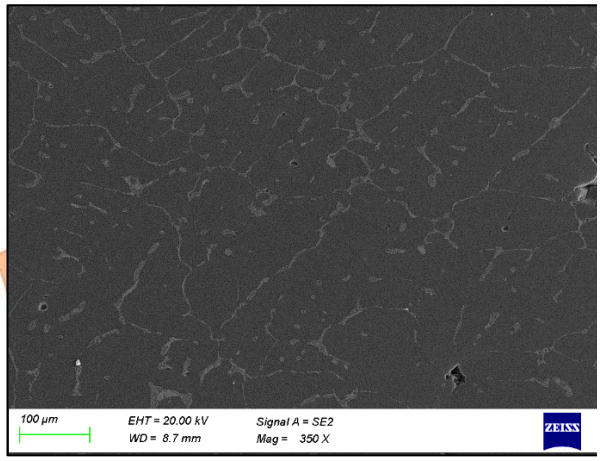

(b) As-cast **Forged**

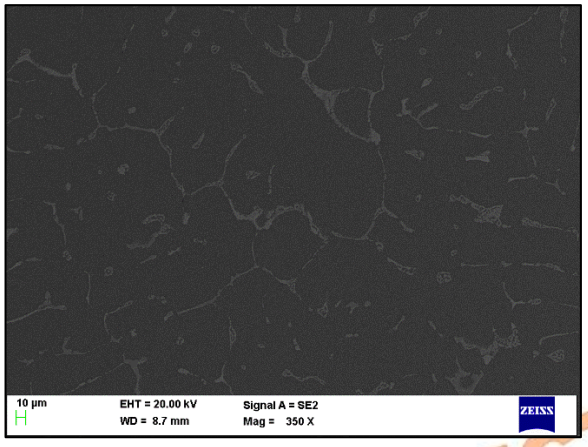

(c) 0.04%Ni +0.2%Sr **HC**

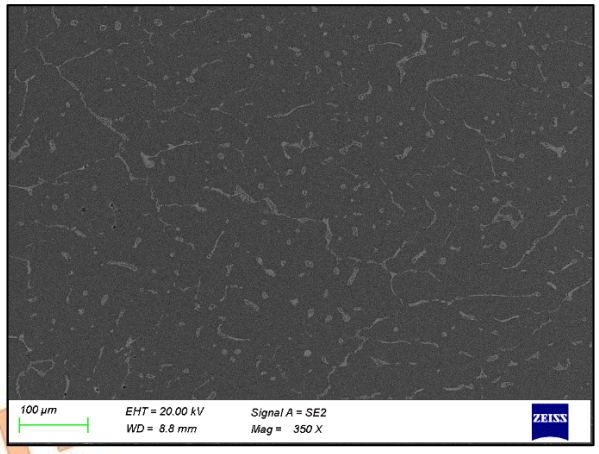

(d) 0.04%Ni +0.2%Sr **FC**

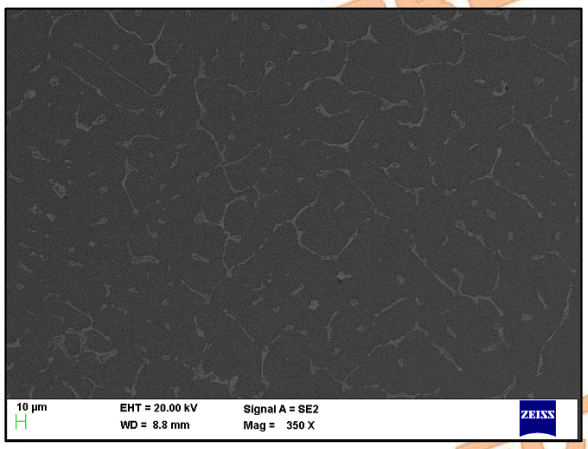

(e) 0.08%Ni +0.2%Sr **HC**

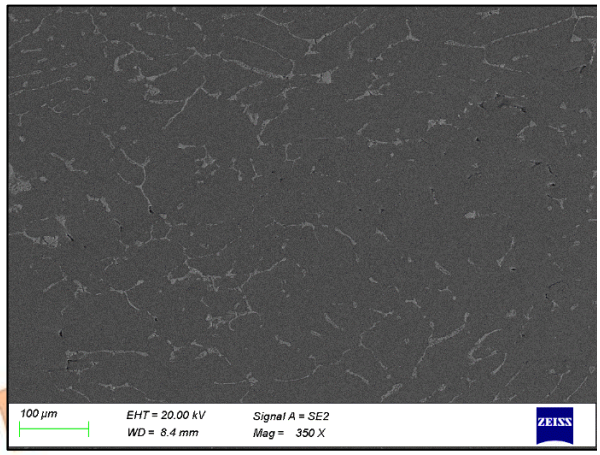

(f) 0.08%Ni +0.2%Sr **FC**

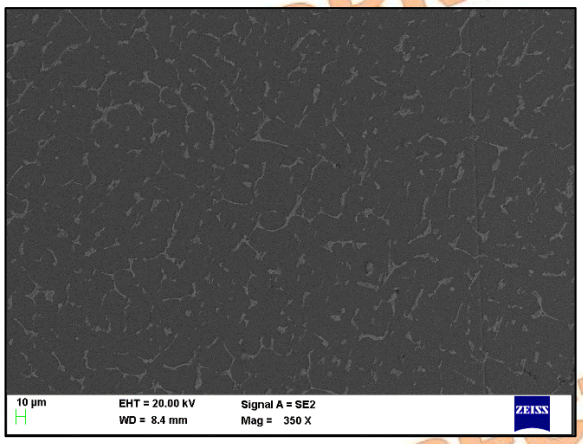

(g) 2%Ni +0.2%Sr **HC**

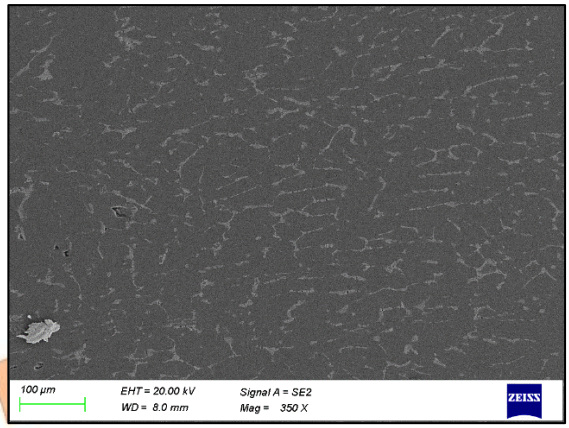

(h) 2%Ni +0.2%Sr **FC**

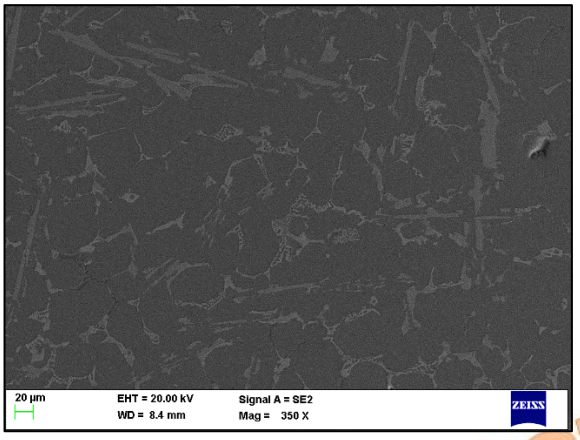

(i) 5%Ni +0.2%Sr **HC**

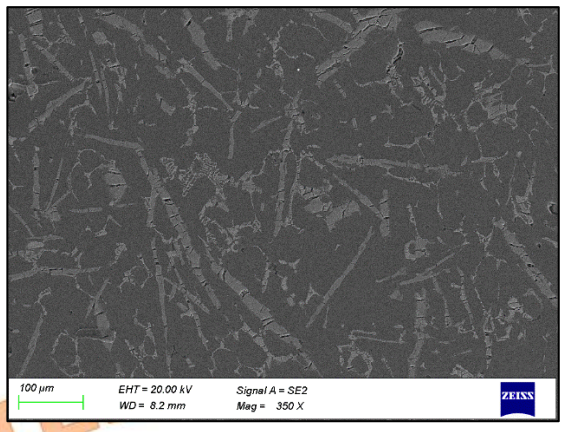

(j) 5%Ni +0.2%Sr **FC**

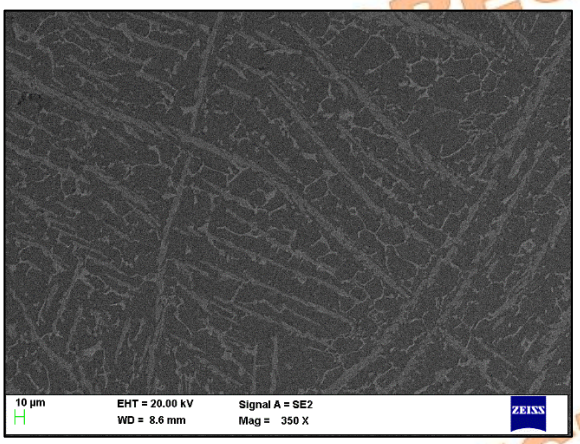

(k) 10%Ni +0.2%Sr **HC**

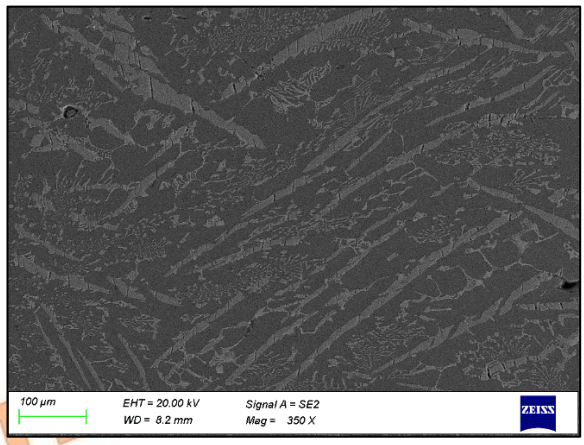

(l) 10%Ni +0.2%Sr **FC**

Fig. 14: SEM Microstructures (350X, 20.0 KV) of **AA 2024** with added varying Ni% and 0.2% of Strontium (Sr) in Homogenized condition (HC) and Forged condition (FC)

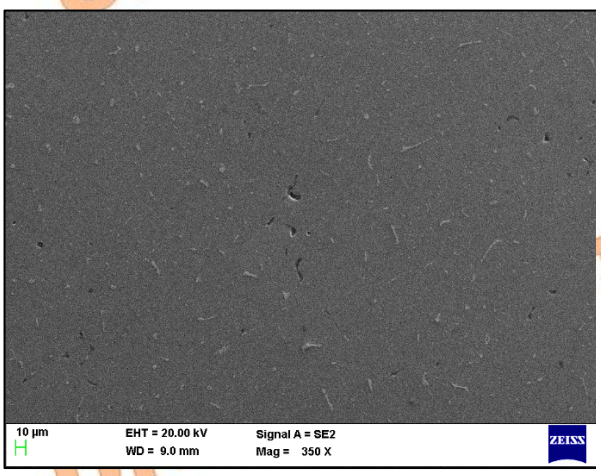

(a) As-cast **Homogenized**

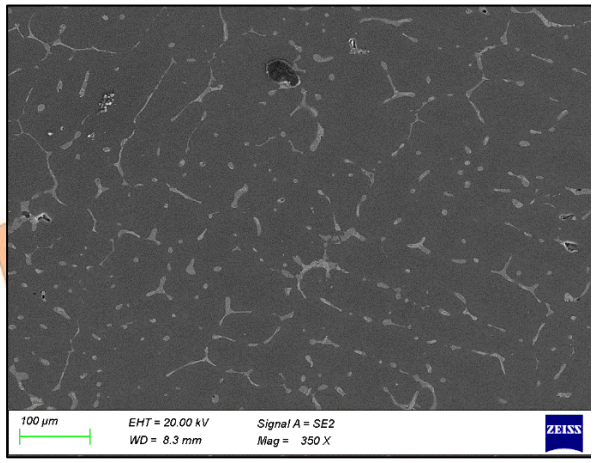

(b) As-cast **Forged**

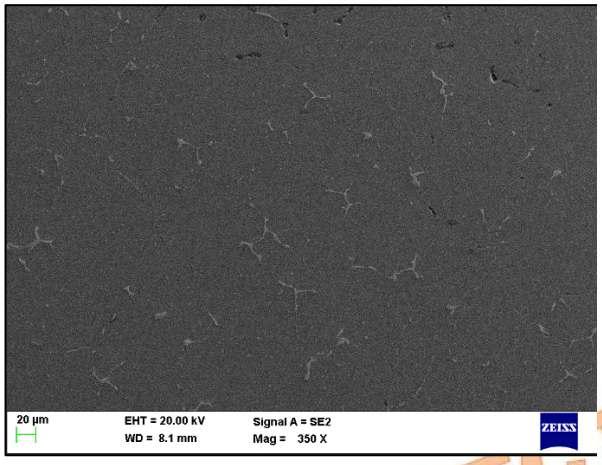

(c) 0.04%Ni +0.2%Sr **HC**

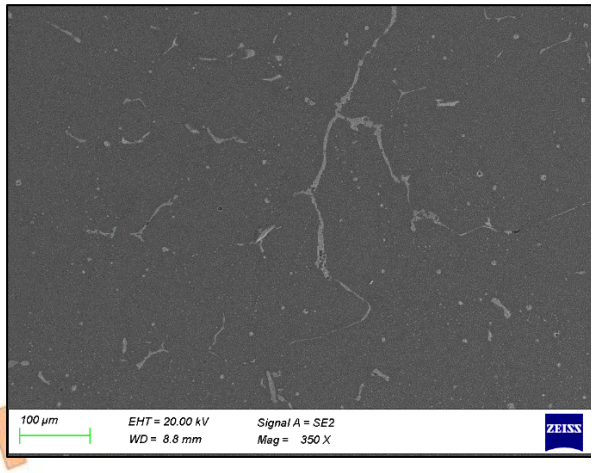

(d) 0.04%Ni +0.2%Sr **FC**

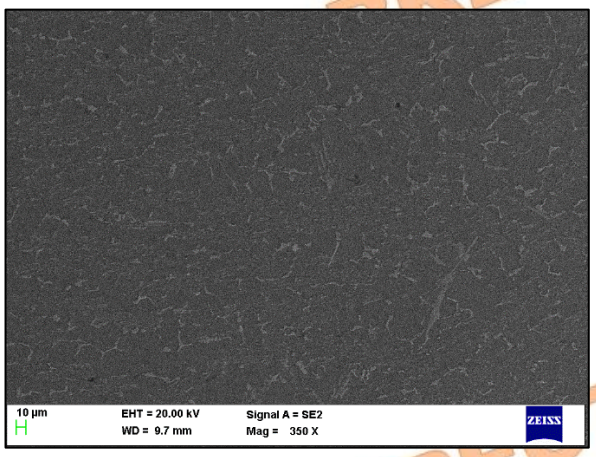

(e) 0.08%Ni +0.2%Sr **HC**

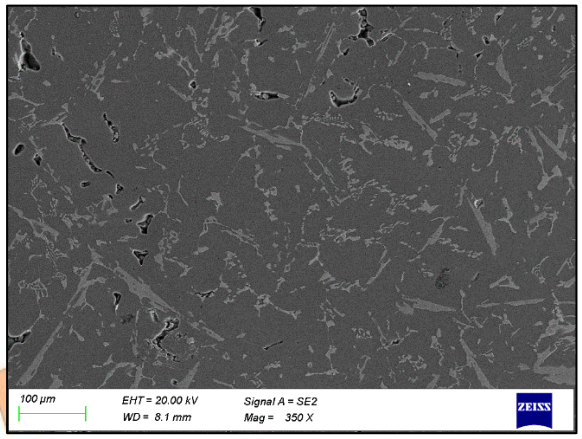

(f) 0.08%Ni +0.2%Sr **FC**

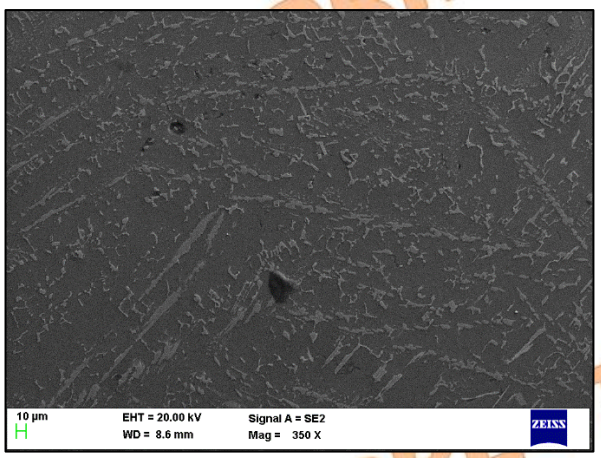

(g) 2%Ni +0.2%Sr **HC**

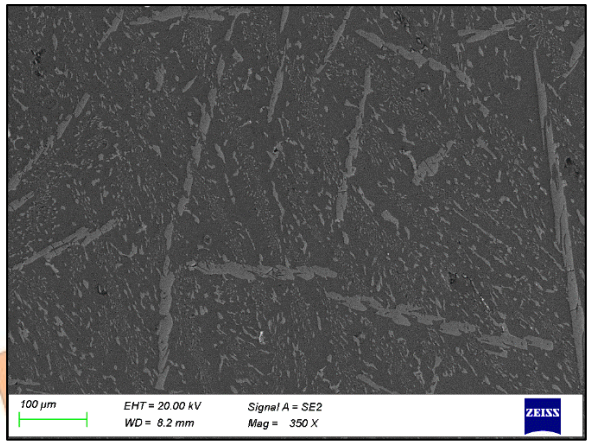

(h) 2%Ni +0.2%Sr **FC**

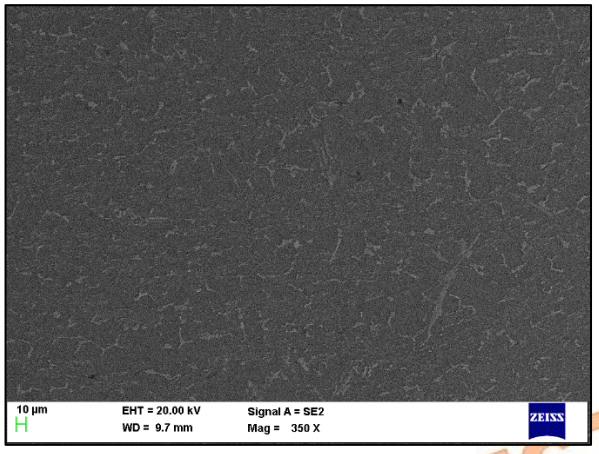

(i) 5%Ni +0.2%Sr **HC**

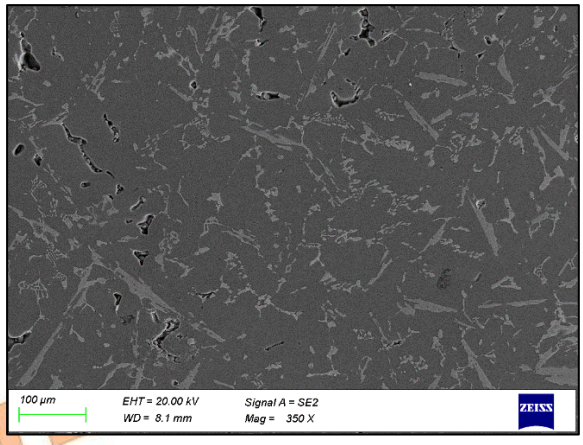

(j) 5%Ni +0.2%Sr **FC**

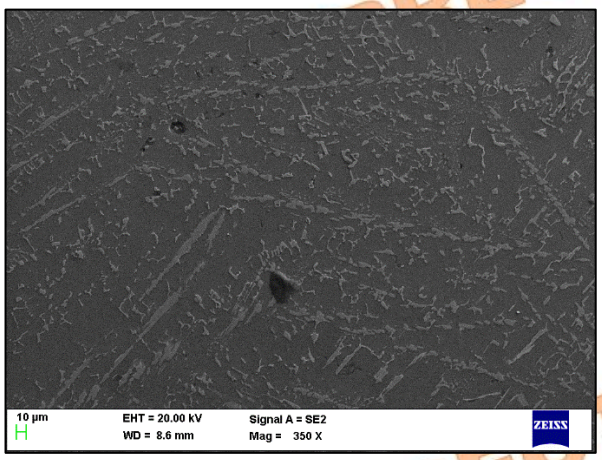

(k) 10%Ni +0.2%Sr **HC**

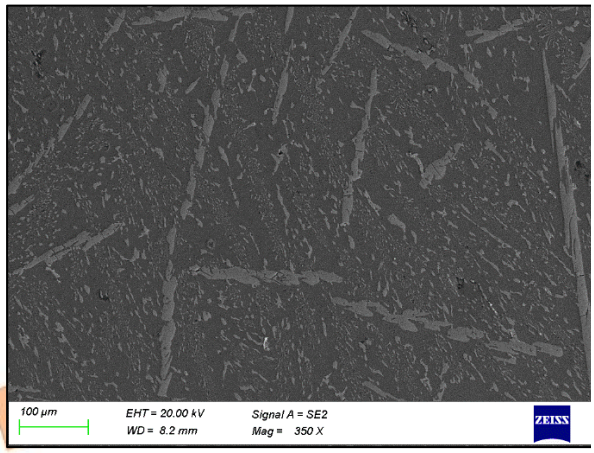

(l) 10%Ni +0.2%Sr **FC**

Fig. 15: SEM Microstructures (350X, 20.0 KV) of **AA 7175** with added varying Ni% and 0.2% of Strontium (Sr) in Homogenized condition (HC) and Forged condition (FC)

3.3. EDS Results

AA 2024 alloy with varying Ni%: EDS data and spectrum are shown in Fig. 16 and Fig. 17 for AA 2024 and AA 7175 alloy added with varying % of Nickel and 0.2% of strontium, respectively. In each figure, the whole area of the extracted SEM image is the selected area.

Figures 16 (a) and (b) show that Cu, Mg, and Al are the significant elements observed in the As-cast and 0.04%Ni added alloy. Similarly, in Fig. 16 (c), a small amount of Fe and Ni were observed apart from the significant alloying elements like Cu, Mg, and Al.

Figure 16 (d) is the EDS results of 2% added Ni, which shows that +1.09wt % and 12.56wt% are observed at the whole area and selected area, respectively; this shows the formation of Ni-Al and Fe-Ni inter-metallic are observed in the specimen. Fig. 16 (e) and (f) show that nearly 18.37wt% and 22.07wt% of nickel are found in the selected region, and hence, nickel aluminum compounds are formed by adding 5% and 10% Ni.

AA 7175 alloy with varying Ni%: EDS data and spectrum are shown in Fig. 17 for AA 7175 alloy added with varying Ni% of Nickel and 0.2% of strontium. It is evident from Figure 17 that Zn, Mg, and Al are the major elements with small amounts of Ni, Cu, and Fe observed for As-cast, 0.04%Ni, and 0.08%Ni added alloy, respectively. EDS results of 2% and 5% said Ni, shown in Fig. 17 (d) and (e), indicate that apart from major alloying elements like Zn, Mg and Al, 33.6wt %Ni, 18.67wt%Ni and 0.36%Sr are observed at the selected area respectively; also Fig. 17 (f) shows EDS of 10%Ni added alloy has 24.63wt%Ni and 2.93wt%Fe; hence, it is evident from these results that there is the formation of Ni-Al and Fe-Ni inter-metallic in the specified specimens. Therefore, nickel aluminum compounds are formed by adding 2%, 5%, and 10 %Ni to Aluminum 7175 alloy.

In both as-cast and homogenized conditions, fine spherical particles of Al3Ni phases are observed in 2%Ni additions and plate-like particles, which look like needle or fibrous structures observed in 5% and 10%Ni additions.

These needle-like structures cannot be fragmented during annealing. However, the smooth planes of Al_3Ni phases are stable for heat treatment up to 600^0C, which proves that the same smooth spherical structures are observed for homogenized and as-cast conditions. The Gibbs free energy consists of three principle components: Surface (Gs), Volume (Gv), and elastic (Ge). Fine eutectics shows enormous interfacial energy, which results in the formation of large particles; in the case of needle-like structure, Gs gets reduced, and Ge is increased, which hinders the process of morphologies [24-25].

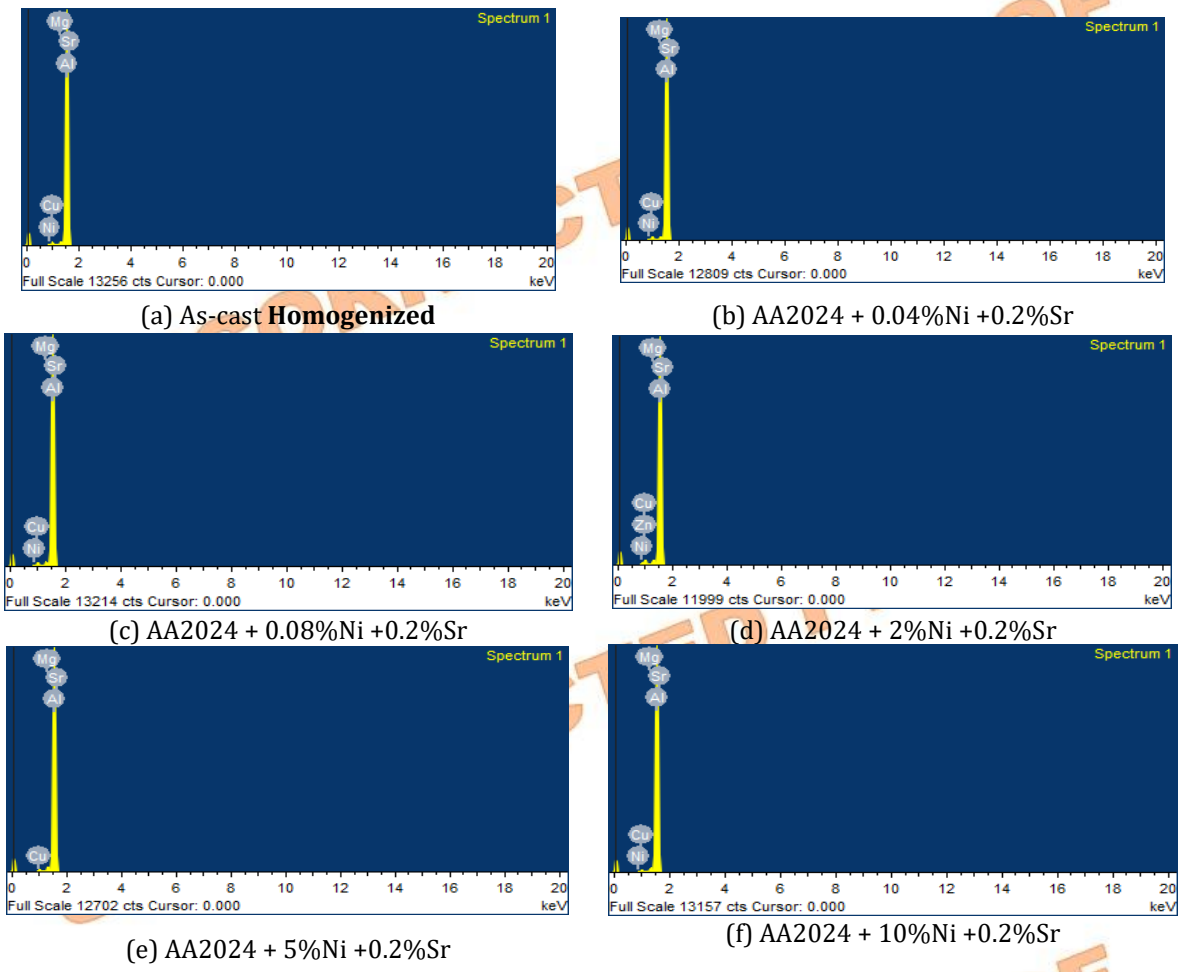

(a) As-cast **Homogenized**

(b) AA2024 + 0.04%Ni +0.2%Sr

(c) AA2024 + 0.08%Ni +0.2%Sr

(d) AA2024 + 2%Ni +0.2%Sr

(e) AA2024 + 5%Ni +0.2%Sr

(f) AA2024 + 10%Ni +0.2%Sr

Fig. 16: EDS plot of AA2024 with added varying Ni% and 0.2% of Strontium (Sr)

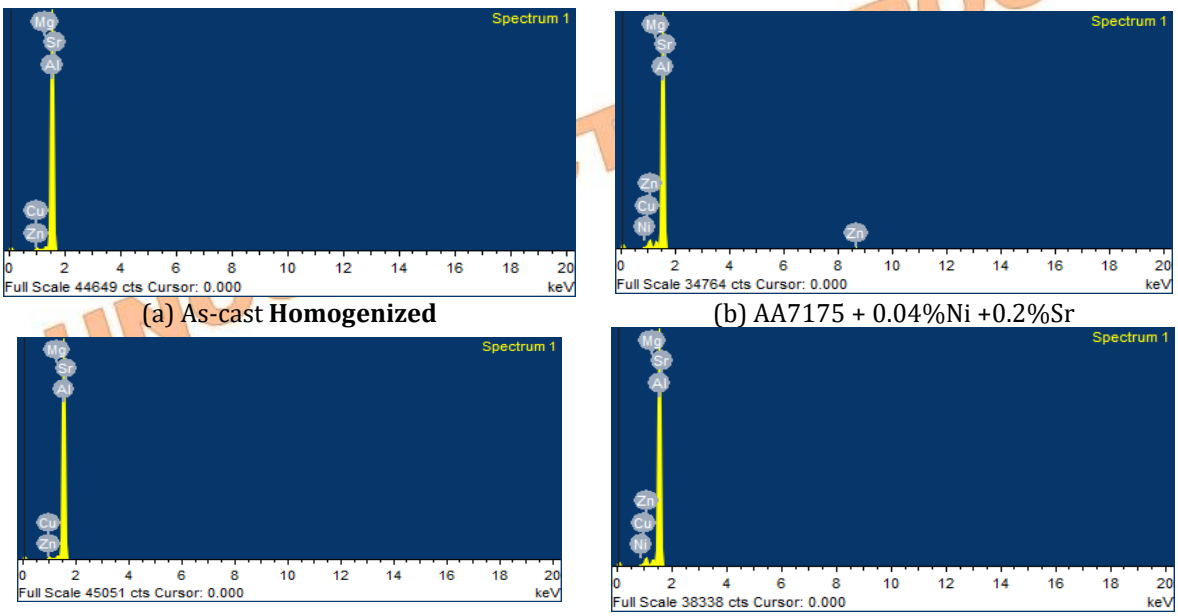

(a) As-cast **Homogenized**

(b) AA7175 + 0.04%Ni +0.2%Sr

(c) AA7175 + 0.08%Ni +0.2%Sr

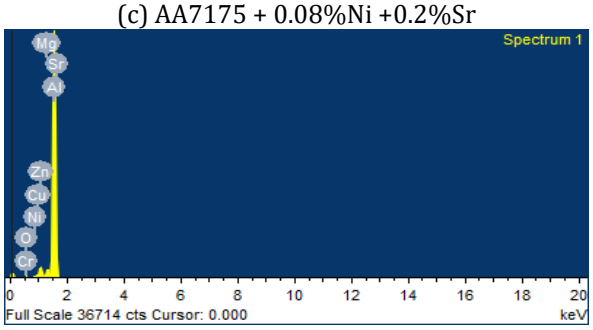

(d) AA7175 + 2%Ni +0.2%Sr

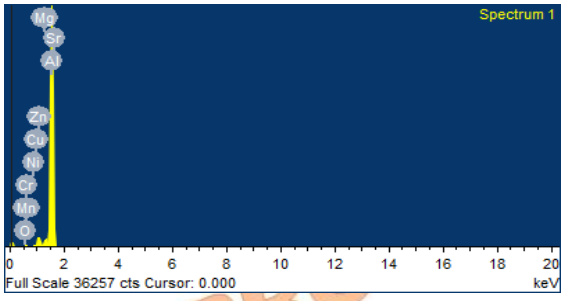

(e) AA7175 + 5%Ni +0.2%Sr

(f) AA7175 + 10%Ni +0.2%Sr

Fig. 17: EDS plot of AA7175 with added varying Ni% and 0.2% of Strontium (Sr)

3.4. XRD Analysis:

It was performed for AA 2024 and AA7175 homogenized alloys with added varying Ni% samples to validate the existence of added nickel in the base alloy. The specimens prepared for SEM were used to analyze XRD as per Fig. 6. The plot of XRD analysis for AA2024 and AA7175 is shown in Fig. 18 and Fig. 19, respectively.

XRD of AA 2024 with varying % of Nickel: The XRD analysis reveals that the intermetallic structures like $\tau Cu_{5.75}Al_{4.5}$, $FeAl_3$, $FeNi_{0.5}Al_{0.5}$, $Fe_{0.1}Al_{0.9}$, $Ni_{0.4}Al_{0.6}$, $Al_{1.1}Ni_{0.9}$, $Ni_{1.16}Al_{0.84}$, $Al_{26}Mg_1Zn_2$, Al-Mg_5, were observed in modified AA 2024 alloys. Aluminum is an FCC structure, $\tau Cu_{5.75}Al_{4.5}$ and Al_3Ni is an orthorhombic crystal structure, $Ni_{0.4}Al_{0.6}$ or Ni_2Al_3 is Nickel Aluminum intermetallic trigonal structure [26]-[28]. The Al_3Ni_2 phase has a hexagonal lattice [24]. $FeAl_3$ is an insoluble phase that helps in improving strength.

From Fig. 18 (a) and (b) with 0.04% and 0.08% Nickel additions, the major compounds of $\tau Cu_{5.75}Al_{4.5}$, Al-Mg-Zn, and $Al_{97}Mn_3$ were observed. However, additional intermetallic compounds of Ni_2Al_3, Ni_3Al, and Fe0.1Al0.9 were observed in Fig. 18 (c), (d), and (e) with 2%, 5%, 10% Nickel additions due to the addition of Nickel more than 1%.

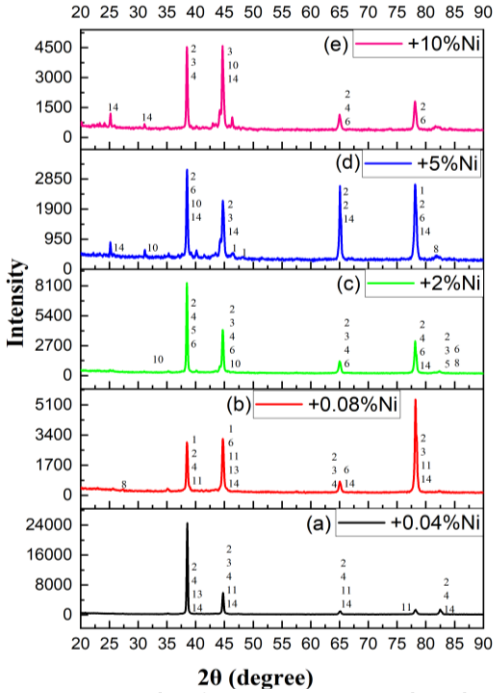

Fig. 18: XRD plot of AA2024-Homogenized Condition

XRD of AA7175 with varying % of Nickel: The XRD analysis reveals that the intermetallic structures like $FeNiAl_2$, $FeAl_3$, $FeAl_6$, Fe_3Ni, $Fe_{0.1}Al_{0.9}$, $NiAl_3$, $Mg_{3.4}Zn_{6.8}Al$, Al-Mg_5, were observed in modified AA 7175 alloys.

From Fig. 19 (a) and (b) with 0.04% and 0.08% Nickel additions, the major compounds of $Mg_{3.4}Zn_{6.8}Al$, Al-Mg_5 were found showing the solid solution of Zinc and magnesium in Aluminum alloy 7175. No major intermetallic compounds were found. However, additional intermetallic compounds of Ni_2Al_3, $NiAl_3$, $Fe_{0.1}Al_{0.9}$, $FeNiAl_2$, $FeAl_3$, $FeAl_6$, Fe_3Ni were observed in Fig. 19 (c), (d) and (e) with 2%, 5%, 10% Nickel additions due to addition of Nickel more than 1%.

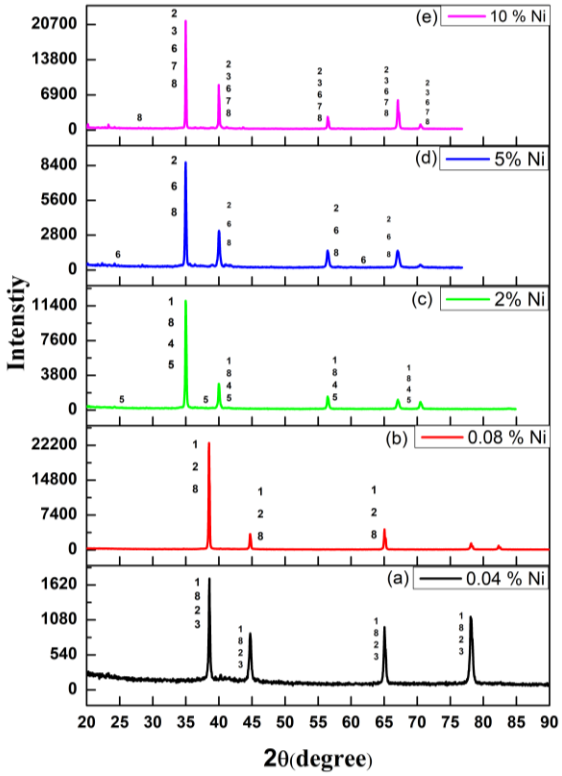

Fig. 19: XRD plot of AA7175-Homogenized

3.5. Coefficient of Thermal Expansion Results

The study compares the displacement and dimensional changes in AA 2024 and AA 7175 alloys with 0.08% and 2% Nickel (Ni) additions. It shows that adding Nickel reduces the coefficient of linear thermal expansion in both alloys. The coefficient decreases from 25.2 to 22.09 µm/m°C in AA 2024 and from 25.56 to 21.94 µm/m°C in AA 7175 with 2% Ni addition, as plotted in Fig. 20.

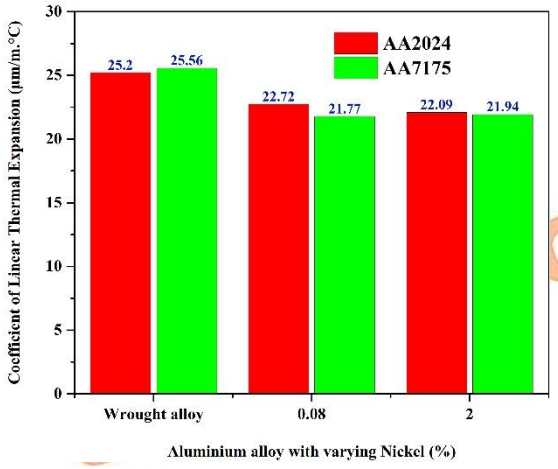

Fig. 20: Comparison of Coefficient of Linear Thermal Expansion of AA2024 & AA7175 Alloys

4. Conclusion

The present study studied the aluminum alloys AA2024 and AA7175 by adding Ni% and 0.20% strontium at As-cast, homogenized, and forged conditions.

- Adding Nickel (Ni) to AA 2024 and AA 7175 alloys improves mechanical and thermal properties up to a certain limit. Tensile strength increases significantly with Ni content up to 5%, showing a 21% improvement for AA 2024 and 80% for AA 7175. However, further additions (e.g., 10% Ni) reduce strength.
- The coefficient of linear thermal expansion decreases with Ni additions, dropping from 25.2 to 22.09 µm/m°C in AA 2024 and from 25.56 to 21.94 µm/m°C in AA 7175 with 2% Ni.
- Microstructural analysis reveals refined grain boundaries with up to 2% Ni, while higher Ni content results in needle-like precipitates and intermetallic phases (Ni_2Al_3, NiAl, $NiAl_3$), which make the alloy brittle. Therefore, 5% Ni is optimal, while 10% Ni is impractical due to the negative effects on material properties.

Equiaxed and fine grains are preferred for optimizing ductility and strength by increasing grain-boundary surface area and evenly distributing grain-boundary constituents. In contrast, coarse, columnar, and feather-like grain structures formed under high thermal gradients with low alloy content negatively impact mechanical properties. The grain type and size are determined by alloy composition, solidification rate, and the availability of effective nucleation sites [30]. It is evident and can be concluded that adding an optimum percentage of 2% Nickel to AA 2024 and AA 7175 alloys is feasible for improving its grains from coarse to fine grains with added intermetallic structures NiAl3 formation, increasing its tensile strength. Conversely, adding 5% and 10% Nickel is not feasible since the formation of fibrous needle shape precipitates.

Inference from the thermal expansion results: The coefficient of linear thermal expansion is reduced from 25.2 to 22.09 µm/m.°C from base alloy to 2% Ni added AA 2024 alloy; similarly, it is reduced from 25.56 to 21.94 µm/m.°C for 2%Ni added AA 7175 alloy. Therefore, adding nickel up to 2% to aluminum alloys is acceptable and helpful in reducing its coefficient of thermal expansion.

Thermal stresses developed in structural parts used in thermal environments, such as heat exchangers, Engines, and turbines [32], which depend on the thermal expansion of the alloy [31]. Hence, a significant reduction in the coefficient of thermal expansion helps reduce thermal stresses. Therefore, materials with lower

thermal expansion can be used in thermal environments. Thus, the prepared AA2024 and AA7175 alloy with 2%Ni additions has lower thermal expansion of 22.09 and 21.94 μm/m.°C, respectively, and could be a possible alloy selection.

Acknowledgment

The authors gratefully acknowledge the Department of Mechanical Engineering, Ramaiah Institute of Technology, for their support in the research. We thank Mr. Yogendra for his support in carrying out the research work. Furthermore, the authors thank the Micro Nano Characterization Facility (MNCF) of IISC Bangalore for their support in utilizing ZEISS ULTRA 55 SEM to capture SEM images. We also acknowledge the Department of Advanced Materials Advanced Materials Laboratory, Ramaiah Institute of Technology, for supporting the extraction of XRD data.

Funding Statement

This research did not receive any specific grant from funding agencies in the public, commercial, or not-for-profit sectors.

Conflicts of Interest

The authors declare no conflict of interest.

References

[1] Erdoğan, A.A., Feyzullahoğlu, E., Fidan, S. and Sinmazçelik, T., 2020. Investigation of erosive wear behaviors of AA6082-T6 aluminum alloy. *Proceedings of the Institution of Mechanical Engineers, Part L: Journal of Materials: Design and Applications*, 234(3), pp.520-530.

[2] Gohardani, O., 2011. Impact of erosion testing aspects on current and future flight conditions. *Progress in Aerospace Sciences*, 47(4), pp.280-303.

[3] Ramesh, C.S., Shreeshail, M.L., Gudi, H.R. and Zulfiqar, K., 2014. Air jet erosion wears behavior of Al6061-SiC-Carbon fibre hybrid composite. In *Materials Science Forum*, vol. 773, pp.547-554.

[4] Yadav, P.K. and Dixit, G., 2019. Investigation of erosion-corrosion of aluminum alloy composites: Influence of slurry composition and speed in a different mediums. *Journal of King Saud University-Science*, 31(4), pp.674-683.

[5] Mohan Raju, S., Ramesha, C.M., Anilkumar, T., Krishna, S., Appaiah, S. and Rajendra, P., 2023. A Study on Grain Refinement of Aluminum Alloys by Adding Grain Refiners and Severe Plastic Deformation: A Review. *Engineering Headway*, 1, pp.3-15.

[6] Martin, J.W., 1998. *Precipitation Hardening*, 2nd ed., Butterworth-Heinemann, Oxford, United Kingdom, pp.79-111.

[7] Zolotorevsky, V.S., Belov, N.A. and Glazoff, M.V., 2007. *Casting Aluminum Alloys*. Elsevier, pp.397-447.

[8] Kaufman, J.G. and Rooy, E.L., 2004. *Aluminum Alloy Castings: Properties, Processes, and Applications*. ASM International.

[9] Patchett, J.A., 1988. The kinetics of the peritectic reactions in aluminum-nickel alloys. *A dissertation to The Graduate School of the University of Florida*.

[10] Jaansalu, K.M. and Distrifcuüon, U., 1998. *Phase Diagram Modelling: Nickel, Aluminum, Chromium System*. Department of National Defence Canada, National Defence Headquarters, DCIEM Air Vehicle Research Detachment.

[11] Pagliarello, A.G., 2011. Effects of modified solution heat treatment on the mechanical properties and stress corrosion cracking susceptibility of aluminum alloy 7075. *PhD diss., Carleton University*.

[12] Starke Jr, E.A. and Staley, J.T., 1996. Application of modern aluminum alloys to aircraft. *Progress in Aerospace Sciences*, 32(2-3), pp.131-172.

[13] ASM Handbook, 1992. *Alloys Phase Diagrams*. The Materials Information Society, Materials Park, Ohio.

[14] Li, H.Y., Li, D.W., Zhu, Z.X., Chen, B.A., Xin, C., Yang, C.L., Zhang, H.Y. and Wei, K., 2016. Grain refinement mechanism of as-cast aluminum by hafnium. *Transactions of Nonferrous Metals Society of China*, 26(12), pp.3059-3069.

[15] Hallem, H., 2005. Precipitation behaviour and recrystallisation resistance in aluminum alloys with additions of hafnium, scandium and zirconium.

[16] Gao, Z., Li, H., Lai, Y., Ou, Y. and Li, D., 2013. Effects of minor Zr and Er on microstructure and mechanical properties of pure aluminum. *Materials Science and Engineering: A*, 580, pp.92-98.

[17] Ghorbani, F., Emamy, M. and Mirzadeh, H., 2021. Enhanced tensile properties of as-cast

Mg-10Al magnesium alloy via strontium addition and hot working. *Archives of Civil and Mechanical Engineering*, 21(2), p.86. doi: 10.1007/s43452-021-00241-3.

[18]Dinnis, C.M., Dahle, A.K., Taylor, J.A. and Otte, M.O., 2004. The influence of strontium on porosity formation in Al-Si alloys. *Metallurgical and Materials Transactions A*, 35, pp.3531-3541.

[19]Sokolowski, J.H., Djurdjevic, M.B., Kierkus, C.A. and Northwood, D.O., 2001. Improvement of 319 aluminum alloy casting durability by high-temperature solution treatment. *Journal of Materials Processing Technology*, 109(1-2), pp.74-180.

[20]Öztürk, İ., Ağaoğlu, G.H., Erzi, E., Dispinar, D. and Orhan, G., 2018. Effects of strontium addition on the microstructure and corrosion behavior of A356 aluminum alloy. *Journal of Alloys and Compounds*, 763, pp.384-391.

[21]Closset, B., Dugas, H., Pekguleryuz, M. and Gruzleski, J.E., 1986. The aluminum-strontium phase diagram. *Metallurgical Transactions A*, 17, pp.1250-1253.

[22]Brook, G.B., 1998. *Smithells Light Metals Handbook*. Elsevier.

[23]Lumley, R., 2011. *Fundamentals of Aluminum Metallurgy: Production, Processing and Applications*. Woodhead Publishing Limited, pp.272.

[24]Zolotorevsky, V.S., Belov, N.A. and Glazoff, M.V., 2007. *Casting Aluminum Alloys*, vol. 12. Elsevier.

[25]Gao, Z., Li, H., Lai, Y., Ou, Y. and Li, D., 2013. Effects of minor Zr and Er on microstructure and mechanical properties of pure aluminum. *Materials Science and Engineering: A*, 580, pp.92-98.

[26]Taylor, A.O. and Doyle, N.J., 1972. Further studies on the nickel–aluminum system. I. β-NiAl and δ-Ni2Al3 phase fields. *Journal of Applied Crystallography*, 5(3), pp.201-209.

[27]Bradley, A.J. and Taylor, U.A., 1937. An X-ray analysis of the nickel-aluminum system. *Proceedings of the Royal Society of London. Series A-Mathematical and Physical Sciences*, 159(896), pp.56-72.

[28]Gunda, N.S.H., Michi, R.A., Chisholm, M.F., Shyam, A. and Shin, D., 2023. First-principles study of Al/Al3Ni interfaces. *Computational Materials Science*, 217, p.111896. doi: 10.1016/j.commatsci.2022.111896.

[29]ASM, 2001. *Specialty Handbook: Aluminum and Aluminum Alloys*, edited by J.R. Davis, ASM International, pp.351-416.

[30]Barron, R.F. and Barron, B.R., 2011. *Design for Thermal Stresses*. John Wiley & Sons.

[31]Mohanraju, S., Ramesha, C.M., Appaiah, S., Kumar, J. and Prasad, N.J.K., 2021. A study on the impact of coefficient of thermal expansion of thermo-mechanical stresses on structural components. *Materials Today: Proceedings*, 46, pp.2528-2533.

[32]Wang, H., Al-amir, Q.R., Jasim, D.J., Ayed, H., Mouldi, A., Deifalla, A. and Mahariq, I., 2024. Enhancing the heat transfer efficiency of an engine heat exchanger through the utilization of an innovative conical braided wire turbulator. *Case Studies in Thermal Engineering*, *61*, p.104873.

[33]Zhou, X., Abed, A.M., Abdullaev, S., Lei, G., He, L., Li, X., Elmasry, Y. and Mahariq, I., 2024. Data-driven study/optimization of a solar power and cooling generation system in a transient operation mode and proposing a novel multi-turbine modification concept to reduce the sun's intermittent effect. *Energy*, *309*, p.133043.

[34]Mohsin, B.B., Abbas, M., Asamoah, J.K.K., Rehman, M.J.U., Umer, M. and Mahariq, I., 2024. A Computational Framework of Marangoni Convective Flow of Trihybrid Nanofluid with Thermo-Bioconvection and Oxytactic Microorganisms Based on the Extended Version of Xue and Yamada-Ota Models.

[35]Fan, G., Paidar, M., Mehrez, S., Ojo, O.O., Liu, M., Dai, Y. and Mahariq, I., 2022. Influence of shoulder diameter on interfacial microstructure and mechanical behavior in dieless friction stir riveting of CP-Copper to 321 stainless steel. *Vacuum*, *197*, p.110809.

[36]Abed, A.M., Chauhan, B.S., Ayed, H., Mouldi, A., Deifalla, A. and Mahariq, I., 2024. Thermodynamic, exergetic and environmental evaluation and optimization of a bio-fuel fired gas turbine incorporated with wind energy derived hydrogen injection. *Case Studies in Thermal Engineering*, *56*, p.104238.

[37]Wang, N., You, K.Y., Mohanavel, V., Mehrez, S., Alamri, S., Nag, K. and Mahariq, I., 2023. Comprehensive study of electromagnetic wave absorption properties of GdMnO3-MoSe2 hybrid composites. *Ceramics International*, *49*(6), pp.9191-9202.